The Asteroid Catalog Using AKARI IRC Slow-Scan Observations

Sunao Hasegawa,[1] Thomas G. Müller,[2] Daisuke Kuroda,[3] Satoshi Takita,[1] and Fumihiko Usui[1]

[1]*Institute of Space and Astronautical Science, Japan Aerospace Exploration Agency, 3-1-1 Yoshinodai, Sagamihara, Kanagawa 229-8510, Japan*
hasehase@isas.jaxa.jp

[2]*Max-Planck-Institut für Extraterrestrische Physik, Giessenbachstraße, 85748 Garching, Germany*

[3]*Okayama Astrophysical Observatory, National Astronomical Observatory, 3037-5 Honjo, Kamogata-cho, Asakuchi, Okayama 719-0232, Japan*

(Received ; accepted)

Abstract

We present an asteroidal catalog from the mid-infrared wavelength region using the slow-scan observation mode obtained by the Infrared Camera (IRC) on-board the Japanese infrared satellite AKARI. An archive of IRC slow-scan observations comprising about 1000 images was used to search for serendipitous encounters of known asteroids. We have determined the geometric albedos and diameters for 88 main-belt asteroids, including two asteroids in the Hilda region, and compared these, where possible, with previously published values. Approximately one-third of the acquired data reflects new asteroidal information. Some bodies classified as C or D-type with high albedo were also identified in the catalog.

Key words: catalogs — infrared: solar system — minor planets, asteroids — space vehicles: instruments

1. Introduction

Physical studies of asteroids provide important information on the present conditions of the solar system. In turn, this can be used to understand the early history and evolution of the solar system. Key data in the physical study of asteroids are reliable geometric albedo and diameter measurements. Geometric albedos place approximate constraints on the surface composition of asteroids (Burbine et al. 2008). The distribution of the geometric albedos of main-belt asteroids provides insight into the chemical and mineralogical evolution of the solar system in the vicinity of the main-belt (Usui et al. ApJ submitted). Combined with estimates

of mass, asteroidal diameter can yield bulk density, which is diagnostic of the internal structure of asteroids (Carry 2012). The size distribution of asteroids can also reveal their original mass and the collisional history of the main-belt asteroids (Bottke et al. 2005).

The radiometric method for determining the geometric albedo and the diameter of asteroids has been used since the early 1970s (Allen 1970), and is a precise method that enables the acquisition of a large amount of data. For example, estimation of the diameter of asteroid (25143) Itokawa using thermal observations is in excellent agreement with subsequent in situ measurements (Müller et al. 2007). Previous studies using the dedicated observations have presented a large amount of data on the geometric albedo and diameter of asteroids, including 84 asteroids by Hansen (1976), 84 asteroids by Morrison (1977), 352 by Gradie & Tedesco (1988), 44 by Fernández et al. (2009), and 101 by Trilling et al. (2010).

The survey that covered the whole sky produced great benefits for study of the asteroids. The Infrared Astronomical Satellite (IRAS; Neugebauer et al. 1984) was launched on January 26, 1983, and mapped >96% of the sky in four wavelength bands during its 10-month mission life. An unbiased catalog of geometric albedo and diameter data for asteroids was established from this all-sky survey (Matson 1986), which ultimately resulted in the geometric albedo and diameter of 2,470 asteroids being presented in the Supplemental IRAS Minor Planet Survey (SIMPS; Tedesco et al. 2002b). Approximately two decades after the IRAS all-sky survey, two infrared astronomical satellites, AKARI (previously known as ASTRO-F; Murakami et al. 2007) and the Wide-field Infrared Survey Explorer (WISE; Wright et al. 2010) performed all-sky surveys in the infrared wavelength region. AKARI was launched on February 21, 2006 and its survey to cover the whole sky in six bands took place over an 18-month mission life. WISE conducted mapping of the whole sky in four bands following its launch on December 14, 2009, which continued until refrigerant expired after eight months. AKARI and WISE acquired geometric albedo and diameter data for 5,120 (Usui et al. 2011) and more than 130,000 asteroids (Grav et al. 2011; Grav et al. 2012; Mainzer et al. 2011; Masiero et al. 2011), respectively.

The radiometric method can obtain geometric albedo and diameter information using not only dedicated observations and the all-sky survey data, but also serendipitous data. The mission purpose of the Midcourse Space Experiment satellite (MSX; Mill et al. 1994), launched on April 24, 1996, was the acquisition of a range of data including an engineering test, an investigation of the composition of Earth's atmosphere, and astronomical research. The MSX infrared astronomy observations were performed to fill a gap in the IRAS all-sky survey observations (Price et al. 2001). Using these data, the geometric albedo and diameter of 168 different asteroids were serendipitously obtained (Tedesco et al. 2002a). The Infrared Space Observatory (ISO; Kessler et al. 1996) was launched on November 17, 1995 and conducted >30,000 individual observations. ISO also carried out parallel and serendipitous observations of the sky whilst the satellite was slewing from one target to the next. The ISOPHOT Serendipity Survey

(ISOSS; Bogun et al. 1996) obtained 170 μm sky brightness data, resulting in 31 asteroids being identified (Müller et al. 2002). The Spitzer Space Telescope (SST; Werner et al. 2004), launched on August 25, 2003, was an observatory type mission like that of ISO and dedicated a significant part of its time to the Legacy programs. Using archive data of the Legacy programs: the First Look Survey-Ecliptic Plane Component (FLS-EPC), the Great Observatories Origins Deep Survey (GOODS), a 24 and 70 μm Survey of the Inner Galactic Disk with MIPS (MIPSGAL), the Spitzer Deep Survey of the HST COSMOS 2-Degree ACS Field (SCOSMOS), the Spitzer Wide-Area Infrared Extragalactic Survey (SWIRE), and Taurus, the serendipitous detection of many small asteroids were conducted (Lonsdale et al. 2003, Meadows et al. 2004, Sanders et al. 2007, Ryan et al. 2009, Bhattachary et al. 2010, Ryan et al. AJ submitted). AKARI was designed as an all-sky survey mission in the infrared region, similar to the IRAS and WISE surveys. However, AKARI had the capability to make pointed observations in addition to its all-sky survey. Approximately 5,000 pointed observations were performed in the cryogenic phase of the AKARI mission before the liquid helium on-board the satellite was exhausted. AKARI is equipped with a 68.5 cm Ritchey-Chrétien type telescope and two scientific instruments: the Far-Infrared Surveyor (FIS; Kawada et al. 2007) and the Infrared Camera (IRC; Onaka et al. 2007). The IRC on-board AKARI was designed to carried out deep photometric imaging and spectroscopy in the pointed observation mode. The IRC can also operate in a scanning operation readout mode that extends the all-sky survey wavelength coverage into the mid-infrared wavelength range (Ishihara et al. 2010). The combination of the scanning operation readout mode and pointed observations allows IRC to make observations of large areas to moderate depth, which is referred to as IRC slow-scan observations (Takita et al. 2012).

Here we present a catalog of the geometric albedo and diameter data for asteroids serendipitously detected by IRC slow-scan observations. We first describe the data processing and catalog creation in Section 2, which is followed by a discussion of the results in Section 3, and a summary of the main findings of this study in Section 4.

2. Data Processing and Catalog Creation

2.1. IRC Slow-Scan Observations

The IRC comprises three cameras (NIR, MIR-S, and MIR-L) that cover wavelength ranges of 2–5, 5–13, and 12–26 μm, respectively. The NIR and two MIR cameras have infrared sensor arrays of 512×412 and 256×256 pixels, and pixel sizes of ca. $1.5''$/pixel and $2.4''$/pixel, respectively. The three cameras have a field of view of ca. $10' \times 10'$, and the NIR and MIR-S cameras share the same field of view through a beam splitter, whereas the MIR-L camera observes the sky at ca. $20'$ away from the other cameras in a direction perpendicular to the AKARI scan direction (Onaka et al. 2007).

The two MIR cameras are able to operate in a scanning operation readout mode (Ishihara et al. 2006), which was developed for the IRC all-sky survey. The NIR camera is not used during the scanning operation readout mode, as the alignment of the NIR array is not suited for all-sky survey observations. The scanning operation readout mode is achieved by operating the MIR cameras in two lines of two-dimensional detector arrays in both continuous and non-destructive readout modes. The sampling rate was set at one sampling per 44 ms of observation time. The MIR-S and MIR-L cameras were operated with filters at *S9W* (reference wavelength: 9.0 μm) and *L18W* (reference wavelength: 18.0 μm) bands, which have effective bandwidths of 4.1 and 10.0 μm in the scanning operation readout mode, respectively.

Although the scanning operation readout mode was developed for the IRC all-sky survey, this mode can also be used for pointed slow-scan observations (Takita et al. 2012). The telescope scanned the sky with much slower speed (8, 15, or 30$''$ s^{-1}) than during the all-sky survey (216$''$ s^{-1}). During slow-scan observations, the telescope scanned along one or two round-trip paths centered about the target position to acquire a redundant dataset. Due to the telescope scan speed and number of round-trip paths, the field of view of IRC slow-scan observations in the scan direction changes from 21.′5 to 2.°9, but perpendicular to the scan direction the field of view varies little (9$'$–14$'$).

IRC slow-scan observations are given in the Astronomical Observation Templates (AOTs) of IRC11 and IRC51. The differences in the AOTs of IRC11 and IRC51 are only the method that enabled examination of the readout signals from the detectors. Pixels were reset at every 51 and 306 samplings to discharge the photo-current for the AOTs of IRC51 and IRC11, respectively. For the IRC11, the detector arrays were operated in the same manner as in the all-sky survey mode, involving binning of 4 pixels in the cross-scan direction. Given that data acquisition of the second line in the array was started at half of the integration time of the first line, the virtual pixel size of IRC11 is 2 pixels (Ishihara et al. 2010). Conversely, the AOT of IRC51 provides full spatial resolution in the cross-scan direction. The full spatial resolution of the IRC with pixel size of 2.″5 in the cross-scan direction was abandoned for the AOT of IRC51, whereas the AOT of IRC11 had a pixel size of 5$''$ after pixel binning.

After the exhaustion of liquid helium on August 26, 2008, the MIR-S and MIR-L cameras could not continue to be operated. IRC slow-scan observations from January 2007 were mainly executed with the AOT of IRC51; consequently, most of the IRC slow-scan observations were made with the AOT of IRC51. Given that the FIS and IRC can be operated simultaneously, 580 IRC slow-scan data (ca. 50 data from the AOT of IRC11 and ca. 530 data from the AOT of IRC51) also include parallel observations from the FIS-dedicated observations. The two cameras with filters at *S9W* and *L18W* acquired 1,040 images in IRC slow-scan observations. All of the IRC slow-scan observations were not actually primarily acquired for the purpose of asteroid research, but rather for other fields of infrared astronomy research. Therefore, only ca. $<$10% of all the IRC slow-scan observations were in the direction of the ecliptic plane.

2.2. Data Reduction Processes

The data packages of the IRC slow-scan observations are stored in dedicated FITS file format, referred to as Time-Series Data (TSD), which were originally developed for the FIS (Takita et al. 2012). The TSD is a binary FITS table and consists of signal output, housekeeping details, and attitude information data for the satellite. Two FITS tables were created from one pointed observation from the MIR-S and MIR-L cameras of the IRC.

The IRC slow-scan observation data were reduced by AKARI data reduction tools (ARIS; Takita et al. 2012), which are written in Interactive Data Language (IDL). Most of the ARIS processing can handle the TSD file formats. The following basic calibrations were applied to the TSD format data in order to correct for the anomalous behavior of the detector output after the reset: non-linearity between incoming photons and output signals, data differentiation, dark subtraction, flat fielding, and masking of bad pixels. Two-dimensional image data were constructed after execution of these basic corrections and calibrations.

IRC slow-scan observational images of the *S9W* and *L18W* in the AOT of IRC11 and *S9W* and *L18W* in the AOT of IRC51 after processing by ARIS have $4\farcs6$/pixel, $5\farcs0$/pixel, $2\farcs3$/pixel, and $2\farcs5$/pixel, respectively. The full width at half maximum sizes of the point spread functions are ca. $8''$ and $10''$ for the AOT of IRC11 and ca. $6''$ and $7''$ for the AOT of IRC51 for the *S9W* and the *L18W* bands, respectively.

2.3. Flux Calibration for Point Sources

The conversion factors for the AOT of IRC51 were derived from relationships between the intensities in ADU from the images and the calculated in-band flux densities in units of Jy for standard stars given in Takita et al. (2012). Since IRC11 is different from IRC51 in the reading method from detectors (Section 2.1), the conversion coefficient of IRC11 should be examined separately. However, Takita et al. (2012) did not derive conversion factors for the AOT of IRC11. Using the same technique to obtain the conversion factors for the AOT of IRC51, the conversion factors for IRC11 were determined as follows.

Infrared observations of two standard stars (Cohen et al. 1999) were used for the absolute flux calibrations of IRC slow-scan observations in the AOT of IRC11 (Table 1). Aperture photometry for the standard stars imaged with MIR-S and MIR-L in the AOT of IRC11 was performed using the APPHOT task of IRAF with a circular aperture radius of 5.2 and 5.3 pixels, respectively. This enabled the sky values for an annulus outside the aperture with a width of 3.5 pixels for the *S9W* band and 3.6 pixels for the *L18W* band to be determined.

The in-band flux densities of the standard stars were taken from Tanabé et al. (2008). The intensities in ADU from the images in the AOT11 are shown in Figure 1 as a function of the predicted in-band flux of the standard stars. A method of the fitting is a method same as Takita et al. (2012). The slopes of the fitted lines in Figure 1 provide the conversion factors for *S9W* and *L18W*. The conversion factors in units of Jy ADU^{-1} for the AOTs of IRC11 and

Table 1. Observed standard stars for in the AOT IRC11

name	RA (J2000)	Dec (J2000)	*S9W* in-band flux [Jy]	*L18W* in-band flux [Jy]
KF09T1	17:59:23.04	+66:02:56.1	3.458×10^{-2}	–
NPM1p67_0536	17:58:54.66	+67:47:36.8	–	3.755×10^{-2}
HD42525	06:06:09.37	−66:02:22.7	2.799×10^{-1}	5.876×10^{-2}

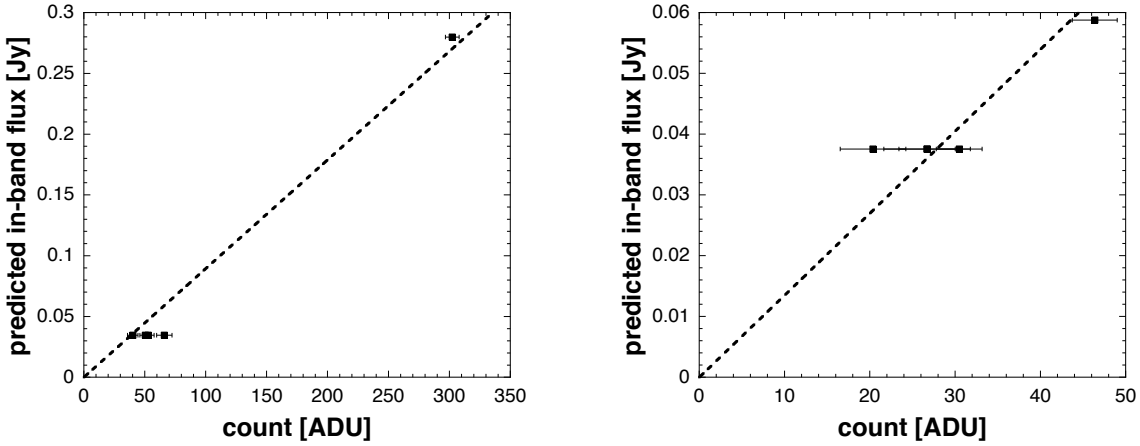

Fig. 1. Relationship between estimated flux density and observed counts of standard stars for the *S9W* (left) and *L18W* (right) bands. The dashed lines in each plot represent a least-squares linear regression of the data.

IRC51 (Table 4 in Takita et al. 2012) are listed in Table 2.

2.4. Asteroidal Search

It is difficult to search for unknown asteroids given the lack of continuity of images obtained from the IRC slow-scan observations. Therefore, a search for known asteroids was performed, involving application of N-body simulations including gravitational perturbations for the Moon, eight planets, (1) Ceres, (2) Pallas, (4) Vesta, and (134340) Pluto to the orbital calculations of asteroids with known orbital elements. The position of the asteroids was calculated using the Runge–Kutta–Nyström 12(10) method (Dormand et al. 1987). The orbital elements for the asteroids used as inputs in the calculations were taken from the Asteroid Orbital Elements Database (Bowell et al. 1994) of Lowell Observatory at the epoch of March 14, 2012. This database contains 544,599 registered asteroids (326,254 numbered and 218,345 unnumbered). The orbital elements of the Sun, planets (including (134340) Pluto), and the Moon were taken from the DE405 JPL Planetary and Lunar Ephemerides in the J2000.0 equatorial coordinates from the NASA Jet Propulsion Laboratory. The parallax between the geocenter and AKARI satellite is not negligible, because AKARI circles in a Sun-synchronous polar orbit at an altitude of 700 km. The observing position of AKARI was adopted in this study, obtained

Table 2. Conversion factors for the IRC slow-scan observations [Jy ADU^{-1}]

Filter band & AOT	Conversion factors	Error
S9W in the AOT11	8.942×10^{-4}	4.845×10^{-5}
S9W in the AOT51	2.518×10^{-4}	3.228×10^{-6}
L18W in the AOT11	1.328×10^{-3}	8.211×10^{-5}
L18W in the AOT51	5.291×10^{-4}	1.365×10^{-6}

by interpolation of data from the AKARI observational scheduling tool, which provides an observing position with sufficient accuracy for the purpose of this study. Taking into account corrections for the light-time, gravitational deflection of light, stellar aberration, and precession and nutation of Earth's rotational axis, calculation of the astronomical coordinates in the search for known asteroids was carried out. In addition, the heliocentric and "AKARI-centric" distance and the phase angle, which are necessary for the thermal models, were calculated. These calculations are similar to those used for the Asteroid catalog using AKARI (AcuA; Usui et al. 2011), which was based on the all-sky survey of AKARI.

Using the acquired IRC slow-scan observational images, information regarding the position, size of the field of view, and observed time can be checked. Based on position and observed time data, known asteroids that should be present in a field of view of a particular image were searched for. The calculated position of a known asteroid is then compared with the position of a point source in the image. If a calculated position includes a point source within $10''$, the point source is considered to be a candidate for that the asteroid. With regards to the thermal flux of the asteroid, a range of brightness is physically restricted in relation to the asteroid albedo, which is typically in the range of 0.01–1.00. If the observed flux of the candidate asteroid matched expected flux range of the known asteroid, then the point source was identified as the asteroid in question.

2.5. Asteroidal Flux Measurements

The AKARI telescope is not able to track moving objects, such as comets and asteroids. Thus, for moving objects, a centroid determination in combination with a standard shift-and-add technique was performed before stacking processing, in order to avoid compromising the photometric accuracy. Aperture photometry for asteroids in the IRC slow-scan observation mode was carried out with the APPHOT task of IRAF using the same aperture radius and sky width as those used in the standard star flux calibrations (Section 2.3 and Takita et al. 2012).

Color differences between the calibration stars (A-type main sequence and K-type giant stars) and asteroids need to be considered, given the wide bandwidth of *S9W* and *L18W*. In order to obtain accurate color-corrected monochromatic flux data, color corrections were applied that were constrained by the shape of spectral energy distributions. As the temperature on the surface of an asteroid changes with the heliocentric distance of the asteroid, the color correction

factor is expressed as a polynomial function of the heliocentric distance of the object (Usui et al. 2011). The color-corrected monochromatic flux $F_{\rm cc}$ in units of Jy, is given by:

$$F_{\rm cc} = \frac{F_{\rm in\text{-}band}}{E_{\rm ccf}}, \tag{1}$$

where $F_{\rm in\text{-}band}$ is the in-band flux in units of Jy. The color correction factor $E_{\rm ccf}$ in each filter band is derived from:

$$E_{\rm ccf} = \begin{cases} 0.984 - 0.0068 R_{\rm h} + 0.031 {R_{\rm h}}^2 - 0.0019 {R_{\rm h}}^3 \ , & \text{for} \quad \textit{S9W}, \\ 0.956 - 0.0024 R_{\rm h} + 0.007 {R_{\rm h}}^2 - 0.0003 {R_{\rm h}}^3 \ , & \text{for} \quad \textit{L18W}, \end{cases} \tag{2}$$

where $R_{\rm h}$ is the heliocentric distance in astronomical units (AU). Given that the filters in the IRC slow-scan observations are the same as those used in the all-sky survey observations, the color correction factors used in our study are the same as those used in the all-sky survey observations (Usui et al. 2011).

2.6. Geometric Albedo and Diameter Determinations by Thermal Modeling

In order to analyze a large amount of thermal infrared asteroid data, a simple thermal model such as the standard thermal model (STM; Lebofsky et al. 1986), isothermal latitude model (ILM; Veeder et al. 1989), or near-Earth asteroid thermal model (NEATM; Harris 1998) is generally applied (Harris & Lagerros 2002). The STM is a simple empirical model that assumes an asteroid is a non-rotating spherical object with zero thermal inertia; consequently, there is no emission on the night side. The thermal emission from a point on the surface of an asteroid is instantaneously in equilibrium with the solar flux absorbed at that point. The ILM is also known as the fast rotating model, and is regarded as a model that makes assumptions that are the opposite to those of the STM. The ILM considers that the surface temperature distribution depends only on latitude, and that the day and night sides contribute equal emissions. The ILM is of most relevance to an asteroid with a high thermal inertia and/or fast rotation. The NEATM model is a modified STM that accounts for cases intermediate between zero (STM) and high thermal inertia (ILM).

In our study, the NEATM was used to determine the geometric albedos and diameters of the observed asteroids. The surface temperature $T(\theta, \varphi)$ is expressed by:

$$T(\theta, \varphi) = \begin{cases} T_{\rm SS} \cdot \sin^{1/4}\theta \cdot \cos^{1/4}\varphi \ , & \text{for} \quad 0 \le \theta \le \pi, \\ 0 \ , & \text{for} \quad \pi \le \theta \le 2\pi, \end{cases} \tag{3}$$

where θ and φ are the longitude and latitude of the asteroid, respectively. The temperature at the sub-solar point $T_{\rm SS}$ in units of kelvin is given by:

$$T_{\rm SS} = \left(\frac{(1 - A_{\rm B}) S_{\rm s}}{\eta \varepsilon \sigma {R_{\rm h}}^2} \right)^{1/4} \ , \tag{4}$$

where $S_{\rm s}$ is the incident solar flux at the heliocentric distance $R_{\rm h}$ = 1 [AU], ε denotes the emissivity at infrared wavelengths (we assume a value of 0.9), σ is the Stefan–Boltzmann constant, and η is the beaming parameter that accounts for the physical quantities related to the surface roughness and thermal inertia of the asteroid. The bolometric albedo $A_{\rm B}$ is given by the equation:

$$A_{\rm B} = p_{\rm v} q \ , \tag{5}$$

where $p_{\rm v}$ and q are the geometric albedo (defined as the ratio of the brightness of an object observed at a zero phase angle to that of a perfectly diffusing Lambertian disk of the same radius located at the same distance) and the phase integral is given by the standard H–G system (Bowell et al. 1989):

$$q = 0.290 + 0.684G \ , \tag{6}$$

where G is the slope parameter. The absolute visual magnitude H is obtained from optical photometry, and allows a diameter D in units of kilometers to be estimated for a given albedo from the following expression (e.g., Pravec & Harris 2007):

$$D = \frac{1329}{\sqrt{p_{\rm v}}}\ 10^{-H/5}, \tag{7}$$

Given that the NEATM is defined at zero phase, a thermal infrared phase coefficient is applied as a function of 0.01 mag deg^{-1} for the NEATM.

Geometry is determined by the heliocentric distance $R_{\rm h}$, the AKARI-centric distance Δ, and the phase angle α used in asteroid identification. The absolute magnitude H and slope parameter G were taken from the dataset of the Lowell Observatory, as was the case for the orbital elements. For error calculations, we assign MPCORB values of Table 3 in Pravec et al. (2012) as uncertainties of for H and 0.10 from Pravec et al. (2012) as it of for G.

The NEATM incorporates a beaming parameter η, which takes into account physical quantities related to the surface roughness and thermal inertia of an asteroid. In the STM, the beaming parameter was held constant at η = 0.756, based on ground-truth occultation observations of the calibrator asteroids. In the ILM model, η is equal to π. As AKARI cannot conduct observations simultaneously in *S9W* and *L18W* bands, default values of η were used.

For the AcuA dataset, η for the 9 μm data and η for the 18 μm data were used, which provide the best match for the sizes and albedos of 55 large main-belt asteroids (Usui et al. 2011). These 55 asteroidal calibrators are distributed between 70 and 1,000 km. Conversely, WISE observed main-belt asteroids between 1 and 1,000 km (Masiero et al. 2011). For main-belt asteroids smaller than 20 km, beaming values are 1.01 $\pm$ 0.16. Masiero et al. (2011) used η = 1.0 for asteroids with only a single thermal band as a reasonable assumption for objects in

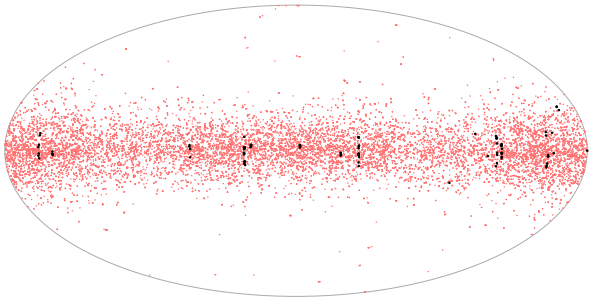

Fig. 2. Distribution of asteroid sightings in ecliptic coordinates. The figure is plotted as a Hammer–Aitoff projection. The red and black dots indicate the asteroids detected by AucA and AcuA-ISS, respectively.

the main-belt. Delbó et al. (2003) also suggested that default values of $\eta = 1.0$ for $\alpha < 30°$ be used for the NEATM. The size range of asteroids observed by Delbó et al. (2003) under $\alpha < 30°$ is 0.1–10 km. Furthermore, Delbó et al. (2007) reported that thermal inertia increases with decreasing size. Hasegawa & Abe (2002) and Ryan & Woodward (2010) concluded that asteroids with smaller diameters have a much greater range of η. These trend in thermal inertia and η can be explained by the differing regolith properties of small and large asteroids. The diameter and phase angle of observed asteroids in the IRC slow-scan observations is mainly in the range of 2–20 km and $\alpha \leq 30°$, respectively. Therefore, all the observed asteroids are assigned $\eta = 1.0$ in our study.

3. Results and Discussion

In total, 89 sightings of 88 different asteroids were identified from IRC slow-scan observational images. Table 3 presents relevant observational details and physical data for the asteroids. The results of the objects included in the catalog are named the Asteroid catalog using AKARI IRC Slow-Scan observations (AcuA-ISS). The asteroid (51250) 2000 JO_{47} was only observed in different epochs at each band (2007/07/04 16:17:06 for *L18W* and 2007/07/05 00:34:24 for *S9W*). All the observed asteroids belong to the main-belt, and include two Hilda asteroids: (13381) 1998 WJ_{17} and (39301) 2001 OB_{100}. Results from the IRC slow-scan observations are given in Table 4, which lists 88 asteroids detected in the mid-infrared region along with their size and albedo data, and associated uncertainties.

Figure 2 shows the asteroids observed by AKARI, with asteroids detected from the all-sky survey (Usui et al. 2011) highlighted in red and those from the IRC slow-scan observations (this study) in black. The 16.32 deg^2 area in the ecliptic plane ($|\beta| \leq 30°$) was observed with the IRC slow-scan observation mode in both the *S9W* and *L18W* filter bands.

Figure 3 shows the distribution of albedos as a function of diameter from the asteroid catalogs of SIMPS, AcuA, WISE, and this study. The detection limits of the IRC slow-scan observations are considered to be 9 mJy for the *S9W* band and 30 mJy for the *L18W* (Takita et al. 2012). The sensitivity of the IRC slow-scan observations is better than that of the

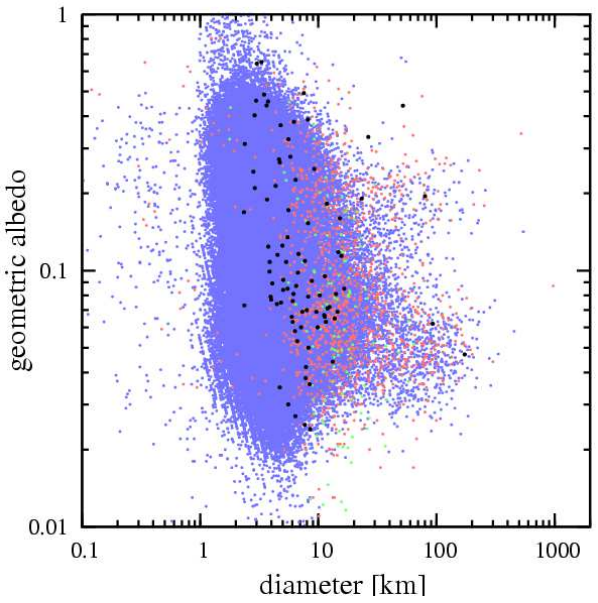

Fig. 3. Distribution of asteroidal diameter and geometric albedo data in the catalogs of SIMPS, AcuA, WISE, and this study (AcuA-ISS). The green, red, blue, and black dots represent the asteroids listed in the SIMPS, AcuA, WISE, and AcuA-ISS catalogs, respectively.

AKARI all-sky survey (Ishihara et al. 2010), but worse than that of the WISE survey (Wright et al. 2010). The detection limits of asteroids observed by the different surveys are consistent with the relative sensitivity of the surveys.

A total of 6, 9, and 56 asteroids detected by our slow-scan observations were previously recorded in the SIMPS, AcuA, and WISE catalogs, respectively. There is no overlap in the ISO and MSX observations (Müller et al. 2002, Dotto et al. 2002, Tedesco et al. 2002a). The geometric albedo and diameter of 29 asteroids in the AcuA-ISS appeared first. All the observed asteroids in the AcuA-ISS catalog should have been originally detected by WISE. However, as WISE was not able to investigate all asteroids in the main-belt at mid-infrared wavelengths (e.g., Figure 1 of Masiero et al. (2011)), these 29 asteroids were not actually observed by WISE.

Figure 4 compares the differences between the geometric albedo and diameter data obtained by IRC slow-scan observations and WISE. The differences are ca. 6% for the diameter and ca. 11% for the geometric albedo. These differences are comparable to the range of the mean error of the asteroids observed by WISE (diameter: 5%; geometric albedo: 21%). Most of the absolute visual magnitudes potentially have large uncertainties, partly due to some hidden light curve effects. The uncertainty on the absolute visual magnitude does not, however, influence the diameter calculation significantly, even though it changes the derived albedos significantly. This accounts for why the differences in albedos are larger than the differences in the diameter data from the various surveys. However, despite this, the IRC slow-scan observational measurements

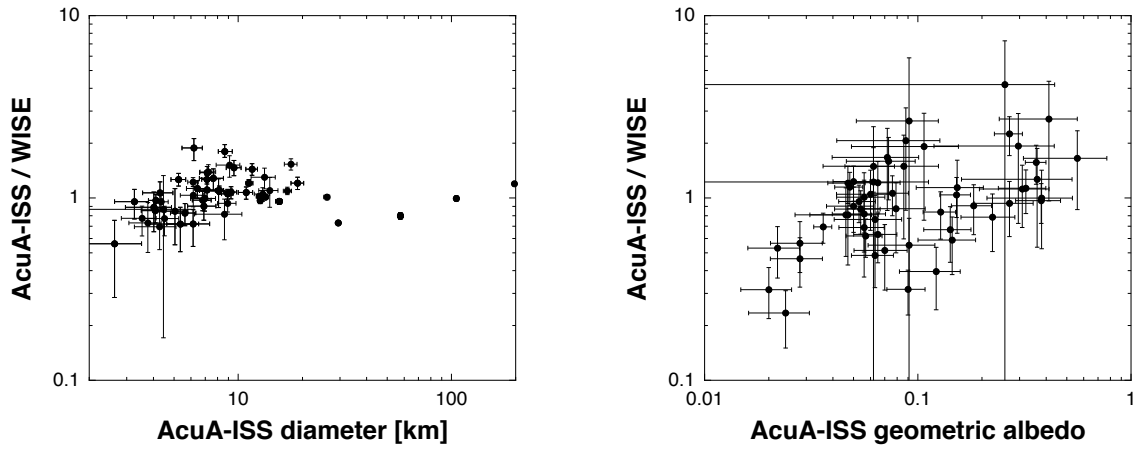

Fig. 4. Comparison between the geometric albedo and diameter data from WISE and the slow-scan observational measurements of this study.

are in good agreement with previous results.

Given that the peak in the incremental number in the AcuA-ISS is ca. 8 km in diameter, main-belt asteroids in the AcuA-ISS were flux limited to an asteroid diameter threshold of >8 km. The cumulative number of asteroids >10 km in size in the AcuA-ISS catalog is 24. WISE observed 7090 asteroids >10 km in diameter (Masiero et al. 2011, Grav et al. 2012). The ratio of detected objects with AcuA-ISS and WISE is $\sim 3 \times 10^{-3}$. Conversely, almost all the asteroids in the AcuA-ISS catalog were detected in $|\beta| \leq 10^{\circ}$. The IRC slow-scan observations were performed to obtain 34 images approximately 26.4 deg^2 in $|\beta| \leq 10^{\circ}$. As the WISE mission life was about 8 months, the size of the survey area in $|\beta| \leq 10^{\circ}$ for WISE is equal to about 9.5×10^3 deg^2. The difference in the observed area between AcuA-ISS and WISE is $\sim 3 \times 10^{-3}$, which as expected is consistent with the detection ratio of AcuA-ISS and WISE given that detection efficiency depends on the search area.

Twenty-six objects in the AcuA-ISS catalog were classified by Tholen (1994), Xu et al. (1995), Bus & Binsel (2002), Lazzaro et al. (2004), and Carvano et al. (2010). The asteroids (12334) 1992 WD_3, (34301) 2000 QO_{171}, and (46072) 2001 EJ belong to the CX spectral type (Carvano et al. 2010). Albedo values suggest that the two asteroids (34301) 2000 QO_{171} and (12334) 1992 WD_3 are M-type and the asteroid (46072) 2001 EJ is C- or P-type. The taxonomic type of the asteroid (16154) Dabramo is X-type (Carvano et al. 2010). However, because the geometric albedo of (16154) Dabramo is >0.1, it is classified as an M-type asteroid. The geometric albedos of the asteroids (2878) Panacea and (13149) Heisenberg are >0.1, but are classed as D- and C-type asteroids, respectively. Mainzer et al. (2012) and Usui et al. (ApJ, submitted) indicated that C- and D-type asteroids having high albedo are present from <50 km in size. Therefore, these asteroids are rare C or D-type asteroids distinguished by high albedos.

Twenty-seven asteroids in the AcuA-ISS catalog belong to the Vesta family (Nesvorný et al. 2006). The spectral type of the two asteroids (2974) Holden and (63717) 2001 QT_{220} are unknown. The geometric albedos of these asteroids are >0.25. Taking into account the high albedo and link to the Vesta family, these asteroids may be V-type.

4. Summary

A serendipitous asteroidal catalog (AcuA-ISS; 88 objects) has been established from slow-scan observations at mid-infrared wavelengths from IRC on the AKARI satellite. The geometric albedo and diameter data for approximately one-third of the asteroids in this new catalog are presented for the first time. The AcuA-ISS catalog provides additional data that supplements previous asteroidal catalogs, such as SIMPS, AcuA, and WISE.

This work is based on observations with AKARI, a JAXA project with the participation of the ESA. We would like to express gratitude to staff of AKARI for their support in generating these observations. This study was partially supported by the Space Plasma Laboratory, ISAS, and JAXA as a collaborative research program.

References

Allen, D. A. 1970, Nature, 227, 158

Bhattachary, S. et al. 2010, ApJ, 720, 114

Bogun, S. et al. 1996, A&A, 315, L71

Bottke, W. F., Durda, D. D., Nesvorný, D., Jedicke, R., Morbidelli, A., Morbidelli, A., Vokrouhlický, D., & Levison, H. F. 2005, Icarus, 179, 63

Bowell, E., Muinonen, K., & Wasserman, L. H. 1994, in Asteroids, Comets, Meteors 1993, ed. A. Milani, M. di Martino, & A. Celino (Dordrecht: Kluwer Academic Publishers), 477

Bowell, E., Hapke, B., Domingue, D., Lumme, K., Peltoniemi, J., & Harris, A. W. 1989, in Asteroids II, ed. R. P. Binzel, T. Gehrels, & M. Shapely (Tucson: University of Arizona Press), 524

Burbine, T. H., Rivkin, A. S., Noble, S. K., Mothé-Diniz, T., Bottke, W. F., McCoy, T. J., Dyar, M. D., & Thomas, C. A. 2008, Rev. Mineral. Geochem., 68, 273

Bus, S. J. & Binzel, R. P. 2002, Icarus, 158, 146

Carry, B. 2012, Planet. Space Sci., in press

Carvano, J. M., Hasselmann, P. H., Lazzaro, D., & Mothe-Diniz, T. 2012, A&A, 510, A43

Cohen, M., Walker, R. G., Carter, B., Hammersley, P., Kidger, M., & Noguchi, K., 1999, AJ, 117, 1864

Delbó, M., dell'Oro, A., Harris, A. W., Mottola, S, & Mueller, M. 2007, Icarus, 190, 236

Delbó, M., Harris, A. W., Binzel, R. P., Pravec, P., & Davies, K. J. 2003, Icarus, 166, 116

Dormand, J. R., El-Mikkawy, M. E. A., & Prince, P. J. 1987, IMA J. Numer. Anal., 7, 423

Dotto E., Barucci, M. A., Müller, T. G., Storrs, A. D., & Tanga, P. 2002, in Asteroids III, ed. W. F. Bottke, A. Cellino, P. Paolicchi, & R. P. Binzel (Tucson: University of Arizona Press), 219

Fernández, Y. R., Jewitt, D., & Ziffer, J. E. 2009, AJ, 138, 240
Gradie, J. & Tedesco, E. F. 1988, Bull. Amer. Astron. Soc., 20, 866
Grav, T. et al. 2011, ApJ, 742, 40
Grav, T. et al. 2012, ApJ, 744, 197
Hansen O. L. 1976, AJ, 81, 74
Harris A. W. 1998, Icarus, 131, 291
Harris A. W. & Lagerros, J. S. V. 2002, in Asteroids III, ed. W. F. Bottke, A. Cellino, P. Paolicchi, & R. P. Binzel (Tucson: University of Arizona Press), 205
Hasegawa, S. & Abe, M. 2002, in Proc. 34th ISAS Lunar Planet. Symp., ed. H. Mizutani & M. Kato (Sagamihara: Institute of Space and Astronautical Science), 91
Ishihara, D. et al. 2006, PASP, 118, 324
Ishihara, D. et al. 2010, A&A, 514, A1
Kawada, M. et al. 2007, PASJ, 59, S389
Kessler, M. F. et al. 1996, A&A, 315, L27
Lazzaro, D., Angeli, C. A., Carvano, J. M., Mothé-Diniz, T., Duffard, R., & Florczak, M. 2004, Icarus, 172, 179
Lebofsky, L. A., Sykes, M. V., Tedesco, E. F., Veeder, G. J., Matson, L. D., Brown, R. H., Gradie, J. C., Feierberg, M. A., & Rudy, R. J. 1986, Icarus, 68, 239
Lonsdale, M. F. et al. 2003, PASP, 810, 897
Mainzer, A. et al. 2011, ApJ, 743, 156
Mainzer, A. et al. 2012, ApJ, 745, 7
Masiero, J. R. et al. 2011, ApJ, 741, 68
Matson, D. L. 1986, IRAS asteroid and comet survey(IPAC, CA)
Meadows, V. S. et al. 2011, ApJS, 154, 469
Mill, J. D. et al. 1994, J. Spacecr. Rockets, 31, 900
Morrison, D. 1977, ApJ, 214, 667
Murakami, H. et al. 2007, PASJ, 59, S369
Müller, T. G., Hotzel, S., & Stickel, M. 2002, A&A, 389, 665
Müller, T. G., Sekiguchi, T., Kaasalainen, M., Abe, M., & Hasegawa, S. 2007, in Proc. IAU Symp. 236, Near Earth Objects, Our Celestial Neighbors: Opportunity and Risk, ed. A. Milani, G. B. Valsecchi, & D. Vokrouhlický (Cambridge: Cambridge University Press), 261
Nesvorný, D., Bottke, W. F., Vokrouhlický, D., Jr., Morbidelli, A., & Jedicke, R. 2006, in Proc. IAU Symp. 229, Asteroids, Comets, Meteors, ed. D. Lazzaro, S. Ferraz-Mello, & J. A. Fernández (Cambridge: Cambridge University Press), 289
Neugebauer G. et al. 1984, ApJ, 278, L1
Onaka, T. et al. 2007, PASJ, 59, S401
Pravec, P. & Harris, A. W. 2007, Icarus, 190, 250
Pravec, P. ,Harris, A. W., Kuŝnirák, P., Galád, D., & Hornoch, H. 2012, Icarus, 221, 365
Price, S. D., Egan, M. P., Carey, S. J., Mizuno, D. R., & Kuchar, T. A 2001, AJ, 121, 2819
Ryan E. L. & Woodward, C. E. 2010, AJ, 140, 933
Ryan E. L. et al. 2009, AJ, 137, 5134

Sanders D. B. et al. 2007, ApJS, 172, 86
Takita, S. et al. 2012, PASJ, 64, in press
Tanabé, T. et al. 2008, PASJ, 60, S375
Tedesco, E. F., Egan, M. P. & Price, S. D. 2002a, AJ, 124, 583
Tedesco, E. F., Noah, P. V., Noah, M., & Price, S. D. 2002b, AJ, 123, 1056
Tholen, D. J. 1984, PhD thesis, Arizona University
Trilling D. E., et al. 2010, AJ, 140, 770
Usui, F. et al. 2011, PASJ, 63, 1117
Veeder, G. J., Hanner, M. S., Matson, D. L., Tedesco, E. F., Lebofsky, L. A., & Tokunaga, A. T. 1989, AJ, 97, 1211
Werner, M. W. et al. 2004, ApJS, 154, 1
Wright, E. L. et al. 2010, AJ, 140, 1868
Xu, S., Binzel, R. P., Burbine, T. H., & Bus, S. J. 1995, Icarus, 115, 1

Table 3. Observational details of the IRC slow-scan mode

NUM	NAME	PROV	Date	$R_{\rm h}$ [AU]	Δ [AU]	α [°]	PID	MODE
43	Ariadne		2006.11.17	2.538602	2.334816	23.16	1500505	IRC11-L
120	Lachesis		2007.8.25	3.297066	3.147807	17.55	1501528	IRC51-S
303	Josephina		2007.5.27	3.227159	3.074105	18.15	1501507	IRC51-L
389	Industria	1894 BB	2007.2.19	2.640165	2.449639	22.33	1500560	IRC51-L
787	Moskva	1914 UQ	2007.1.19	2.678289	2.490071	21.34	1500536	IRC51-L
1223	Neckar	1931 TG	2007.1.19	2.993022	2.818871	19.04	1500536	IRC51-S
1671	Chaika	1934 TD	2007.7.19	3.167706	3.010767	18.77	1501520	IRC51-S
2727	Paton	1979 SO9	2007.2.18	2.611124	2.417393	21.98	1500552	IRC51-S
2878	Panacea	1980 RX	2007.7.17	2.826768	2.633587	20.44	1501516	IRC51-S
2974	Holden	1955 QK	2007.7.19	2.410074	2.194508	25.12	1501520	IRC51-S
3380	Awaji	1940 EF	2006.12.19	2.799506	2.627247	20.75	1500520	IRC11-L
3454	Lieske	1981 WB_1	2007.2.18	2.506598	2.310919	22.99	1500552	IRC51-L
3525	Paul	1983 CX_2	2007.5.25	3.350142	3.209716	17.71	1501502	IRC51-L
4508	Takatsuki	1990 FG_1	2007.5.25	2.107394	1.856114	29.25	1501501	IRC51-S
5031	Svejcar	1990 FW_1	2007.8.25	2.734255	2.557551	21.47	1501525	IRC51-L
5414	Sokolov	1977 RW_6	2006.11.18	2.654776	2.478728	21.47	1500513	IRC11-L
5921		1992 UL	2007.5.27	2.101870	1.853744	28.56	1501507	IRC51-L
6113	Tsap	1982 SX_5	2007.1.19	2.831880	2.652805	20.01	1500537	IRC51-L
7279	Hagfors	1985 VD_1	2007.7.17	2.589649	2.391503	22.91	1501513	IRC51-L
7514		1986 ED	2007.2.19	2.659431	2.470582	22.14	1500560	IRC51-L
7859	Lhasa	1979 US	2006.11.18	2.522808	2.330671	22.63	1500513	IRC11-S
8040	Utsumikazuhiko	1993 SY_3	2006.11.16	2.387672	2.188442	24.50	1500506	IRC11-L
8801		1981 EQ_{29}	2007.2.19	3.046047	2.882508	19.11	1500561	IRC51-L
9429	Porec	1996 EW_1	2007.1.19	3.251622	3.097513	17.39	1500537	IRC51-L
10224	Hisashi	1997 UK_{22}	2006.12.19	2.790197	2.615382	20.77	1500520	IRC11-L
10442	Biezenzo	4062 T-1	2007.5.25	3.237080	3.087467	18.18	1501504	IRC51-L
10906		1997 WO_{44}	2007.1.18	2.065941	1.824184	27.53	1500538	IRC51-S
11296	Denzen	1992 KA	2007.5.27	2.680008	2.491249	22.08	1501507	IRC51-L
12206		1981 EG_{27}	2007.1.19	2.845371	2.667759	19.91	1500537	IRC51-L
12334		1992 WD_3	2006.11.17	2.032610	1.767803	29.39	1500505	IRC11-S
12411	Tannokayo	1995 SQ_3	2007.2.19	2.146342	1.908209	27.86	1500560	IRC51-L
13149	Heisenberg	1995 EF_8	2007.2.18	3.298470	3.153460	17.31	1500552	IRC51-L
13381		1998 WJ_{17}	2007.2.19	4.215680	4.098958	13.65	1500561	IRC51-L
13445		3063 P-L	2007.1.18	3.298641	3.163087	16.94	1500538	IRC51-L
14147	Wenlingshuguang	1998 SG_{43}	2006.11.17	2.341921	2.120256	25.50	1500504	IRC11-L

Table 3. (Continued.)

NUM	NAME	PROV	Date	R_h [AU]	Δ [AU]	α [°]	PID	MODE
15746		1991 PN_8	2006.11.17	2.670670	2.477771	21.97	1500505	IRC11-L
16154	Dabramo	2000 AW_2	2007.1.18	3.321473	3.186623	16.86	1500538	IRC51-L
23916		1998 SD_{131}	2007.2.18	3.056860	2.891344	18.57	1500553	IRC51-S
24389		2000 AA_{177}	2007.5.25	2.429128	2.218058	24.81	1501502	IRC51-S
29027		7587 P-L	2007.2.19	2.290763	2.062212	26.01	1500560	IRC51-S
29352		1995 JR	2007.7.19	2.530867	2.333805	23.79	1501520	IRC51-L
29664		1998 WY_{23}	2007.2.19	2.738363	2.548114	21.38	1500561	IRC51-S
31062		1996 TP_{10}	2007.8.25	3.127006	2.965808	18.78	1501527	IRC51-S
34218		2000 QC_{78}	2007.1.20	2.640249	2.461623	21.87	1500546	IRC51-L
34301		2000 QO_{171}	2006.11.17	2.731269	2.545068	21.57	1500504	IRC11-L
34676		2000 YF_{126}	2006.9.21	3.453976	3.315299	16.91	1710038	IRC51-L
37345		2001 SV_{153}	2007.8.25	3.377545	3.241115	17.19	1501526	IRC51-L
38120		1999 JN_{39}	2007.5.25	1.923790	1.645326	32.59	1501501	IRC51-S
39301		2001 OB_{100}	2007.7.19	4.500299	4.400443	13.07	1501520	IRC51-L
44191		1998 LF_2	2007.1.20	2.625713	2.446439	21.92	1500546	IRC51-L
46072		2001 EJ	2007.1.19	2.959495	2.783794	19.28	1500536	IRC51-S
48571		1994 ER_5	2007.2.19	2.327067	2.108739	25.59	1500560	IRC51-L
49402		1998 XZ_{44}	2007.8.25	2.528788	2.331854	23.08	1501528	IRC51-L
51250		2000 JO_{47}	2007.7.4	2.918787	2.749098	19.32	1602431	IRC51-S
51250		2000 JO_{47}	2007.7.5	2.919128	2.745111	19.30	1602428	IRC51-L
52265		1985 RM_3	2007.1.19	2.508926	2.306929	22.90	1500536	IRC51-L
55883		1997 WF_8	2006.11.16	2.389337	2.186822	25.17	1500503	IRC11-S
57208		2001 QB_{57}	2007.1.19	2.272077	2.049657	25.85	1500545	IRC51-L
57481		2001 ST_{153}	2006.12.19	2.288468	2.067001	25.66	1500520	IRC11-S
58011		2002 TW_{280}	2007.5.25	3.001184	2.837739	19.63	1501504	IRC51-L
58748		1998 FB_9	2007.1.19	2.718304	2.535665	21.36	1500545	IRC51-L
58798		1998 FU_{100}	2007.2.19	3.116269	2.956199	18.63	1500561	IRC51-L
63717		2001 QT_{220}	2007.2.19	2.203776	1.971396	26.89	1500561	IRC51-L
63887		2001 SH_3	2007.8.25	3.207130	3.051977	18.06	1501528	IRC51-S
74318		1998 UB_{16}	2007.8.25	3.001487	2.842352	19.51	1501525	IRC51-L
79087	Scheidt	1977 UM_2	2007.1.20	2.167639	1.945359	27.89	1500543	IRC51-L
81955		2000 PT_{18}	2007.1.19	2.943009	2.774224	19.67	1500545	IRC51-L
85871		1999 BN_{30}	2007.2.28	2.298378	2.082549	25.72	1600365	IRC51-L
93418		2000 SB_{305}	2007.1.18	2.619743	2.441709	21.43	1500538	IRC51-L
93798		2000 WP_{45}	2007.1.18	2.821893	2.660610	20.49	1500535	IRC51-L
94193		2001 BN_7	2007.5.27	3.066873	2.905949	19.16	1501507	IRC51-L

Table 3. (Continued.)

NUM	NAME	PROV	Date	$R_{\rm h}$ [AU]	Δ [AU]	α [°]	PID	MODE
109898		2001 SE_{20}	2006.11.18	3.305919	3.169253	17.12	1500513	IRC11-L
114424		2002 YE_{36}	2006.11.16	2.163698	1.942199	28.08	1500503	IRC11-L
116491		2004 BU_{12}	2007.5.25	3.096796	2.940222	19.35	1501501	IRC51-L
119811		2002 AC_{156}	2006.11.17	2.746422	2.558025	21.29	1500505	IRC11-L
130992		2000 WT_{159}	2007.8.25	2.344822	2.128820	25.45	1501527	IRC51-L
131490		2001 SJ_{164}	2007.8.25	2.762148	2.585283	21.03	1501528	IRC51-L
135859		2002 TS	2006.11.18	2.387461	2.186881	24.04	1500513	IRC11-L
139668		2001 QB_{194}	2006.11.17	2.318870	2.094051	25.56	1500505	IRC11-L
140692		2001 UF_{65}	2007.1.20	2.676858	2.497344	22.09	1500543	IRC51-S
141308		2001 YT_{119}	2007.1.20	2.910120	2.750073	19.72	1500546	IRC51-L
147957		1993 TM_{21}	2006.11.16	2.147420	1.918652	28.33	1500503	IRC11-S
150620		2000 YM_{71}	2006.11.16	2.550888	2.361453	22.75	1500506	IRC11-S
150739		2001 QA_{67}	2006.12.19	2.412085	2.202069	24.31	1500520	IRC11-S
155875		2001 DR_{91}	2007.1.19	2.984466	2.814412	18.98	1500537	IRC51-L
157836		1998 FG_{102}	2007.1.18	2.249671	2.031143	25.02	1500538	IRC51-S
162143		1998 VJ_1	2007.7.4	2.065237	1.804591	27.61	1602429	IRC51-S
249789		2000 XC_{53}	2006.11.17	2.565457	2.360142	23.14	1500504	IRC11-S
253116		2002 UX_{69}	2007.3.7	1.919815	1.648152	31.59	3160010	IRC51-S

Notes. NUM, NAME, and PROV in the table refer to the number, name, and provisional designation of the asteroid, respectively. $R_{\rm h}$, Δ, and α are the heliocentric distance, the AKARI-centric distance, and the phase angle, respectively. PID is the pointed ID for AKARI. Usually it is identical with the Target ID, but is different for parallel mode observations. MODE indicates the AOT and filter band. "-S" and "-L" in MODE mean the *S9W* and the *L18W* bands, respectively.

Table 4. Geometric albedo and diameter data for asteroids detected by IRC slow-scan observations

NUM	NAME	PROV	H [mag]	G	D [km]	σ_D [km]	$p_{\rm v}$	$\sigma_{p_{\rm v}}$	S	A	W
43	Ariadne		7.93	0.11	57.56	1.68	0.359	0.040	1	1	1
120	Lachesis		7.75	0.15	197.13	2.74	0.036	0.004	1	1	1
303	Josephina		8.80	0.15	105.36	0.54	0.048	0.007	1	1	1
389	Industria	1894 BB	7.88	0.15	89.15	0.28	0.157	0.015	1	1	0
787	Moskva	1914 UQ	9.70	0.15	29.42	0.28	0.269	0.040	1	1	1
1223	Neckar	1931 TG	10.58	0.15	26.07	0.86	0.152	0.025	0	1	1
1671	Chaika	1934 TD	12.10	0.15	13.29	1.71	0.145	0.043	0	0	1
2727	Paton	1979 SO9	12.10	0.15	8.92	0.88	0.321	0.080	0	0	1
2878	Panacea	1980 RX	11.70	0.15	17.00	0.76	0.128	0.022	0	0	1
2974	Holden	1955 QK	13.10	0.15	6.15	0.75	0.269	0.082	0	0	1
3380	Awaji	1940 EF	12.00	0.15	8.35	0.92	0.402	0.107	0	0	0
3454	Lieske	1981 WB_1	13.20	0.15	7.13	0.38	0.183	0.039	0	0	1
3525	Paul	1983 CX_2	12.10	0.15	16.64	0.59	0.092	0.015	0	1	0
4508	Takatsuki	1990 FG_1	13.50	0.15	3.54	0.64	0.560	0.229	0	0	1
5031	Svejcar	1990 FW_1	14.00	0.15	8.92	0.54	0.056	0.014	0	0	1
5414	Sokolov	1977 RW_6	12.70	0.15	6.90	1.03	0.309	0.109	0	0	1
5921		1992 UL	13.60	0.15	4.11	0.31	0.379	0.090	0	0	1
6113	Tsap	1982 SX_5	13.10	0.15	13.40	0.36	0.057	0.011	0	1	1
7279	Hagfors	1985 VD_1	12.90	0.15	12.67	0.29	0.076	0.014	0	0	1
7514		1986 ED	13.50	0.15	9.82	0.44	0.073	0.015	0	0	0
7859	Lhasa	1979 US	13.30	0.15	12.66	0.65	0.053	0.011	1	0	0
8040	Utsumikazuhiko	1993 SY_3	13.70	0.15	5.14	0.64	0.221	0.069	0	0	0
8801		1981 EQ_{29}	13.30	0.15	5.35	1.35	0.296	0.159	0	0	1
9429	Porec	1996 EW_1	13.30	0.15	11.61	0.73	0.063	0.014	0	0	1
10224	Hisashi	1997 UK_{22}	14.10	0.15	6.14	1.36	0.107	0.053	0	0	1
10442	Biezenzo	4062 T-1	12.90	0.15	15.57	0.54	0.050	0.010	0	0	1
10906		1997 WO_{44}	13.70	0.15	3.77	0.64	0.412	0.159	0	0	1
11296	Denzen	1992 KA	13.20	0.15	6.43	0.68	0.224	0.063	0	0	1
12206		1981 EG_{27}	14.70	0.15	6.81	0.59	0.050	0.014	0	0	0
12334		1992 WD_3	13.80	0.15	6.14	0.34	0.142	0.035	0	0	1
12411	Tannokayo	1995 SQ_3	13.70	0.15	3.29	0.52	0.539	0.197	0	0	0
13149	Heisenberg	1995 EF_8	13.70	0.15	5.29	1.62	0.209	0.134	0	0	0
13381		1998 WJ_{17}	12.20	0.15	18.98	1.29	0.065	0.015	0	0	1
13445		3063 P-L	12.60	0.15	15.94	0.56	0.063	0.012	0	0	0
14147	Wenlingshuguang	1998 SG_{43}	13.70	0.15	4.02	0.95	0.363	0.184	0	0	1

Table 4. (Continued.)

NUM	NAME	PROV	H [mag]	G	D [km]	σ_D [km]	$p_{\rm v}$	$\sigma_{p_{\rm v}}$	S	A	W
15746		1991 PN_8	14.40	0.15	5.54	0.70	0.100	0.034	0	0	0
16154	Dabramo	2000 AW_2	12.30	0.15	10.41	0.83	0.196	0.048	0	0	0
23916		1998 SD_{131}	13.40	0.15	15.00	1.30	0.034	0.009	0	0	0
24389		2000 AA_{177}	14.20	0.15	7.25	0.61	0.070	0.019	0	0	1
29027		7587 P-L	14.90	0.15	3.11	1.33	0.200	0.177	0	0	0
29352		1995 JR	14.40	0.15	5.95	0.58	0.087	0.026	0	0	0
29664		1998 WY_{23}	13.10	0.15	9.11	1.14	0.122	0.038	0	0	1
31062		1996 TP_{10}	12.00	0.15	17.68	1.21	0.090	0.018	0	1	1
34218		2000 QC_{78}	14.30	0.15	3.20	1.25	0.328	0.266	0	0	0
34301		2000 QO_{171}	14.10	0.15	4.86	1.35	0.172	0.103	0	0	0
34676		2000 YF_{126}	13.70	0.15	11.21	0.43	0.047	0.009	0	0	1
37345		2001 SV_{153}	13.60	0.15	10.90	0.83	0.054	0.013	0	0	1
38120		1999 JN_{39}	15.40	0.15	4.35	0.34	0.065	0.018	0	0	1
39301		2001 OB_{100}	12.70	0.15	16.77	1.62	0.052	0.014	0	0	0
44191		1998 LF_2	15.00	0.15	5.42	0.69	0.060	0.020	0	0	0
46072		2001 EJ	13.60	0.15	8.62	2.09	0.086	0.045	0	0	1
48571		1994 ER_5	15.20	0.15	4.96	0.48	0.060	0.018	0	0	0
49402		1998 XZ_{44}	14.20	0.15	8.15	0.37	0.056	0.013	0	0	1
51250		2000 JO_{47}	13.30	0.15	13.02	1.08	0.050	0.012	0	0	1
51250		2000 JO_{47}	13.30	0.15	12.61	0.41	0.053	0.010	0	0	1
52265		1985 RM_3	15.20	0.15	4.30	0.69	0.079	0.031	0	0	1
55883		1997 WF_8	14.60	0.15	6.11	0.77	0.068	0.023	0	0	0
57208		2001 QB_{57}	14.60	0.15	4.08	0.53	0.153	0.052	0	0	1
57481		2001 ST_{153}	14.70	0.15	6.62	0.63	0.053	0.016	0	0	0
58011		2002 TW_{280}	13.80	0.15	9.25	0.62	0.062	0.016	0	0	1
58748		1998 FB_9	14.70	0.15	5.05	0.85	0.091	0.037	0	0	1
58798		1998 FU_{100}	13.80	0.15	7.64	0.98	0.091	0.031	0	0	1
63717		2001 QT_{220}	15.00	0.15	2.63	1.09	0.256	0.220	0	0	1
63887		2001 SH_3	13.00	0.15	14.06	1.43	0.056	0.015	0	0	1
74318		1998 UB_{16}	14.00	0.15	7.57	0.87	0.078	0.025	0	0	0
79087	Scheidt	1977 UM_2	14.10	0.15	3.26	0.58	0.381	0.160	0	0	1
81955		2000 PT_{18}	14.70	0.15	7.14	0.82	0.046	0.015	0	0	1
85871		1999 BN_{30}	15.00	0.15	3.22	0.45	0.171	0.061	0	0	0
93418		2000 SB_{305}	15.50	0.15	7.15	0.56	0.022	0.006	0	0	1
93798		2000 WP_{45}	15.20	0.15	8.65	0.65	0.020	0.005	0	0	1
94193		2001 BN_7	14.40	0.15	6.96	0.92	0.063	0.022	0	0	1

Table 4. (Continued.)

NUM	NAME	PROV	H [mag]	G	D [km]	σ_D [km]	$p_{\rm v}$	$\sigma_{p_{\rm v}}$	S	A	W
109898		2001 SE_{20}	14.40	0.15	8.09	1.39	0.047	0.019	0	0	1
114424		2002 YE_{36}	14.80	0.15	5.59	0.38	0.068	0.018	0	0	0
116491		2004 BU_{12}	14.60	0.15	9.54	0.76	0.028	0.008	0	0	1
119811		2002 AC_{156}	14.70	0.15	5.63	0.75	0.073	0.025	0	0	1
130992		2000 WT_{159}	15.90	0.15	5.25	0.41	0.028	0.008	0	0	1
131490		2001 SJ_{164}	14.50	0.15	6.81	0.69	0.060	0.018	0	0	1
135859		2002 TS	15.70	0.15	6.20	0.67	0.024	0.007	0	0	1
139668		2001 QB_{194}	14.70	0.15	7.39	0.34	0.043	0.010	0	0	0
140692		2001 UF_{65}	14.30	0.15	9.23	1.07	0.040	0.013	0	0	0
141308		2001 YT_{119}	15.00	0.15	4.23	1.38	0.099	0.068	0	0	0
147957		1993 TM_{21}	15.70	0.15	2.59	1.37	0.139	0.150	0	0	0
150620		2000 YM_{71}	15.40	0.15	4.46	2.47	0.062	0.070	0	0	1
150739		2001 QA_{67}	14.70	0.15	8.73	0.62	0.031	0.008	0	0	0
155875		2001 DR_{91}	15.00	0.15	9.65	0.62	0.019	0.005	0	0	0
157836		1998 FG_{102}	15.20	0.15	4.51	0.81	0.072	0.031	0	0	1
162143		1998 VJ_{1}	15.10	0.15	4.28	0.92	0.088	0.043	0	0	1
249789		2000 XC_{53}	14.60	0.15	8.78	0.97	0.033	0.010	0	0	0
253116		2002 UX_{69}	16.60	0.15	2.60	0.23	0.060	0.017	0	0	1

Notes. H and G are the absolute magnitude and slope parameter taken from the Asteroid Orbital Elements Database of the Lowell Observatory, respectively. D and $p_{\rm v}$ are the calculated diameter and geometric albedo of the asteroids, respectively. σ_D and $\sigma_{p_{\rm v}}$ are the uncertainties on D and $p_{\rm v}$, respectively, estimated from the thermal model calculations. S, A, and W indicate whether the asteroid was detected by IRAS (Tedesco et al. 2002b), AKARI (Usui et al. 2011), or WISE (Masiero et al. 2011, Grav et al. 2012), respectively.